# Journal Pre-proof

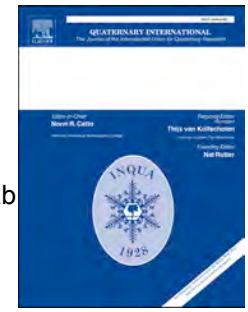

Environmental effects caused by the Mw 8.2, September 8, 2017, and Mw 7.4, June 23, 2020, Chiapas-Oaxaca (Mexico) subduction events: Comparison of large intraslab and interface earthquakes

M. Magdalena Velázquez-Bucio, Maria Francesca Ferrario, Eliana Muccignato, Sabina Porfido, Aadityan Sridharan, Kervin Chunga, Franz Livio, Sundararaman Gopalan, Alessandro M. Michetti

PII: S1040-6182(21)00569-3

DOI: https://doi.org/10.1016/j.quaint.2021.11.028

Reference: JQI 9048

To appear in: *Quaternary International*

Received Date: 14 May 2021

Revised Date: 23 November 2021

Accepted Date: 29 November 2021

Please cite this article as: Velázquez-Bucio, M.M., Ferrario, M.F., Muccignato, E., Porfido, S., Sridharan, A., Chunga, K., Livio, F., Gopalan, S., Michetti, A.M., Environmental effects caused by the Mw 8.2, September 8, 2017, and Mw 7.4, June 23, 2020, Chiapas-Oaxaca (Mexico) subduction events: Comparison of large intraslab and interface earthquakes, *Quaternary International* (2021), doi: https://doi.org/10.1016/j.quaint.2021.11.028.

# Environmental effects caused by the Mw 8.2, September 8, 2017, and Mw 7.4, June 23, 2020, Chiapas-Oaxaca (Mexico) subduction events: Comparison of large intraslab and interface earthquakes

M. Magdalena Velázquez-Bucio [a,*], Maria Francesca Ferrario [a], Eliana Muccignato [a], Sabina Porfido [b,c], Aadityan Sridharan [d], Kervin Chunga [e], Franz Livio [a], Sundararaman Gopalan [f], Alessandro M. Michetti [a,c]

[a] Dipartimento di Scienza e Alta Tecnologia, Università degli Studi dell'Insubria, Via Valleggio 11, 22100 Como, Italy

[b] ISA-CNR, via Roma, 64, 83100 Avellino, Italy

[c] Osservatorio Vesuviano—INGV, 80124 Napoli, Italy

[d] Department of Physics, Amrita Vishwa Vidyapeetham, Amritapuri, India

[e] Departamento de Construcciones Civiles, Facultad de Ciencias Matemáticas, Físicas y Químicas, Universidad Técnica de Manabí, UTM, Av. José María Urbina, Portoviejo 130111, Ecuador

[f] Department of Electronics and Communication Engineering, Amrita Vishwa Vidyapeetham, Amritapuri, India

* Corresponding author.

E-mail addresses: magda_vb@yahoo.com.mx, mm.velazquezbucio@uninsubria.it (M.M. Velázquez-Bucio).



## Abstract

Earthquake Environmental Effects (EEEs) such as surface faulting, landslides, liquefaction and tsunamis are widely distributed following strong seismic events and may account for a significant part of the overall damage. Here, we investigate EEEs generated by two earthquakes with different source parameters, both occurring along the Mexican subduction zone: the Sept. 8, 2017, Mw 8.2, moderate depth, normal fault, intraslab event; and the June 23, 2020, Mw 7.0, shallow depth, thrust fault, interface event. We document all the EEEs for each event, assign an intensity value using the Environmental Seismic Intensity (ESI-2007) scale, and derive the macroseismic fields. Finally, we compute the attenuation of intensity with distance and we compare it with other subduction zone earthquakes worldwide, demonstrating the repeatability of EEEs. This work represents the first application of the

ESI-2007 scale to an intraslab earthquake and documents its wide applicability in different seismotectonic settings. We argue that EEEs provide useful information that should not be neglected in seismic hazard assessment procedures.

Keywords: Earthquake Environmental Effects; Intensity attenuation; ESI-2007 scale; September 8, 2017 Chiapas earthquake; June 23, 2020 Oaxaca earthquake

## 1. Introduction

Strong earthquakes commonly produce a variety of environmental effects, which may worsen the societal impact of the earthquake itself and account for a significant part of the overall damage. The type, number and dimension of Earthquake Environmental Effects (EEEs) provide valuable information for characterizing the pattern of damage and for improved seismic hazard assessment (Papanikolaou 2011, Serva et al., 2016, Ferrario et al., 2020). EEEs can be classified in a systematic way through the Environmental Seismic Intensity (ESI-2007) scale (Michetti et al., 2007; Serva et al., 2016; Caccavale et al., 2019; Huayong, et al., 2019; King et al., 2019; Silva et al., 2019; Porfido et al., 2020). The analysis of EEEs offers the opportunity to integrate and complement data obtained by means of other intensity scales more focused on damage affecting the built environment.

Here, we investigate two earthquakes that occurred along the Mexican subduction zone, a region characterized by high seismicity rates and capable of generating Mw > 8 earthquakes. The subduction of the Cocos plate beneath the North American one is the main process controlling the location and parameters of seismic sources throughout Mexico. In addition to interface earthquakes, shallow crustal and intraslab earthquakes are also generated in this setting (Zúñiga et al., 2017; Sahakian et al., 2018; Suárez et al., 2020). The two investigated earthquakes occurred on September 8, 2017, in the offshore Gulf of Tehuantepec (Mw 8.2, focal depth 45.9 km; *Servicio Sismológico Nacional*, 2017); and on June 23, 2020, with epicenter close to La Crucecita (Mw 7.4; focal depth 22.6; *Servicio Sismológico Nacional*, 2020; Fig. 1).

The September 8, 2017 earthquake is an intraslab event, with normal focal mechanism, with high magnitude and a relatively deep hypocenter. From 1929 to 2017 only seven normal faulting intraslab earthquakes of Mw> 7.6 are available worldwide (e.g., 1977, Sumba earthquake; 2007, Mw 8.1 Kuril Islands earthquake; 2009, South of Samoa earthquake;

1933 Mw 8.5 Sanriku earthquake; Okal et al., 2016ñ Melgar et al., 2018). They are typically related to bending stresses in the outer rise of the subduction zone.

By contrast, the June 23, 2020 earthquake occurred along the subduction interface and had a reverse focal mechanism. It is characterized by a lower magnitude and a shallower hypocenter with respect to the 2017 Gulf of Tehuantepec earthquake. These two events, by their nature and location, represent major earthquakes which eventually affect the center and south of the Mexican country, and Central America (Fig. 1).

The main goal of this work is the analysis of EEEs generated by these two events. For the September 8, 2017 event, we carried out field reconnaissance surveys immediately after the earthquake. For the June 23, 2020 event, given the restrictions due to the COVID-19 pandemic, it was not possible to perform fieldwork. For this reason, the inventory is based exclusively on information collected remotely, namely a meticulous search on scientific literature, social networks, newspapers, and newscasts, complemented with landslide mapping from satellite images.

We assign an ESI-2007 value for each documented EEEs, then we draw isoseismal maps. The 2017 Tehuantepec earthquake is the first intraslab earthquake ever studied using the ESI-2007 scale. By comparing the dimension and spatial distribution of EEEs generated by the two events, we evaluate the applicability of the ESI-2007 scale for subduction events with different source parameters. We compute the attenuation of ESI-2007 with distance for the two investigated events and we compare it with other subduction zone earthquakes worldwide, and with the attenuation along the Mexican subduction zone obtained from Modified Mercalli (MM) intensities.

The comprehensive evaluation of the seismic risk in a given region should take into consideration all the possible seismogenic sources and structural settings. We argue that the analysis of either intraslab and interface events, and of effects on the built as well as on the natural environment is critical for a better assessment of the seismic hazard along the Mexican subduction zone.

## 2. Regional setting

### 2.1. Seismotectonics

Mexico is located in a seismically active region, due to convergence of five tectonic plates (i.e., North America, Caribbean, Cocos, Pacific and Rivera; Fig. 1). Both interface and

intraplate earthquakes are generated in this region. Specifically, the subduction of the Cocos plate beneath the North American one is the main process controlling the seismicity throughout the country, with the most seismically active zones located in central and southwest Mexico (Chen et al., 2018). According to Suárez et al. (2020), mainly three types of earthquakes occur in southern Mexico. The largest and most frequent are the interface earthquakes, at a depth between 5 and 35 km. Less frequently, intraslab normal-faulting earthquakes can occur, at depths between 50 and 180 kilometers. Intraslab normal-faulting events, like the September 8, 2017 are considered rare (Okal et al., 2016; Melgar et al., 2018). They express the bending associated with the downward deflection of the slab below the overlying plate (Okal et al., 2016). The third type is represented by earthquakes of maximum magnitude in the order of Mw 7.2, produced in the shallow crust of the Trans-Mexican Volcanic Belt, and typically characterized by normal or transtensional focal mechanisms.

In this paper, we analyze two earthquakes that occurred in the Gulf of Tehuantepec (Fig. 1), a region showing some peculiar features within the Mexican subduction zone (Suárez et al., 2019; Melgar et al., 2020). The most outstanding one is a remnant fracture zone called Tehuantepec Ridge (TR; Fig. 1), which separates the Cocos plate in two parts of different ages. Moreover, the TR corresponds to the point where the Cocos Plate changes from a sub-horizontal dip beneath the center of Mexico to ~ 45° dip beneath the Southern Mexico (Ye et al., 2017; Suárez et al., 2019, Velasco et al., 2020). The TR produces a large diversity of stress regimes and faulting styles (Sahakian et al., 2018). In this region the subduction rate is ~ 6.4-7.5 cm/yr (Singh et al., 2000; DeMets et al., 2010; Ye et al., 2017), increasing from north to south (Melgar et al., 2020).

### 2.2. Historical seismicity

According to the National Seismological Service of Mexico (SSN, *Servicio Sismológico Nacional;* SSN catalog), four earthquakes of M ≥ 8 have occurred in the territory of Mexico, along the subduction zone, between 1900 and 2020. The most recent is that one of September 8, 2017 (Mw 8.2). Prior to this event, other earthquakes occurred on June 3, 1932 (Mw 8.2), September 19, 1985, (Mw 8.1), and October 9, 1995 (Mw 8.0); all these 3 earthquakes occurred along the subduction interface. There is additional evidence of a

major subduction earthquake, occurred in 1787, on the coasts of Oaxaca and Guerrero, which reached a macroseismically estimated magnitude between 8.4 and 8.6 (Suárez and Albini, 2009).

Approximately 25% of the seismic activity of the national territory is recorded in the State of Oaxaca (*Servicio Sismológico Nacional*, 2020), which is also the state most heavily affected by the September 8, 2017, and June 23, 2020, earthquakes. Earthquakes of M7 have been systematically recorded since the implementation of the instrumental seismic record in Mexico. However, where the September 8, 2017, earthquake occurred, there is no record of large earthquakes since 1902; consequently, this region has been identified as a seismic gap (Singh et al., 1981; Suárez et al., 2019). The occurrence of a possible Mw 8,4-8.6 megathrust earthquake in 1787, in the Gulf of Tehuantepec, suggests the possibility of future events in the area, which would have devastating consequences (Suárez et al., 2019).

## 3. The 2017 and 2020 earthquakes

### 3.1. The September 8, 2017 Gulf of Tehuantepec earthquake

The Mw 8.2, September 8 earthquake occurred offshore, in the Gulf of Tehuantepec (Lat. 14.76 N; Long. -94.11 W; Fig. 1), at a focal depth of 45.9 km, 140 km SW of Pijijiapan, Chiapas, at 04:49:19.2 UTC (23:49:18 local time), with a source duration of 75 seconds (Jiménez, 2018). It is an intraslab earthquake with a normal-faulting focal mechanism (focal plane 1: strike = 314, dip = 73, rake = -100; focal plane 2: strike = 164, dip = 20, rake = -61; USGS, 2017).

The earthquake caused the release of the cumulated extensional stress associated with the flexure of the slab on the plate of Cocos and the preferred fault plane from moment-tensor solutions, is a steep normal fault with strike N314. The mainshock ruptured unilaterally to the NW at a relatively high speed (Ye et al., 2017; Chen et al. 2018; Segou and Parsons, 2018). The length of rupture extended ~180 km to the NW along the coast of Oaxaca, and from a depth of ca. 30 to 70 km, with a maximum slip of ~13 m (Ye et al., 2017; Chen et al., 2018). In the fifteen days following the mainshock, 4326 aftershocks were recorded; the largest were the Mw 5.8, September 8, 2017, and the Mw 6.1, September 23, 2017, earthquakes (*Servicio Sismológico Nacional*, 2017; SSN, website). According to Ye et al.

(2017), this is the largest intraslab earthquake documented throughout the Mexican subduction zone during the instrumental period and, given that source parameters and rupture dynamics of similar events worldwide are poorly understood (Ye et al., 2017; Melgar et al., 2018), it is a challenge to evaluate their seismic potential.

Numerous localities, especially small towns and rural communities suffered structural damage and environmental effects. Due to the high energy and intermediate focal depth, the associated environmental effects extend over a relatively large area, which requires a study with a systematic approach to data collection, to show a complete scenario of the extent and impact of such an event, in terms of intensity.

### 3.2. The June 23, 2020, La Crucecita earthquake

On June 23, 2020, at 15:29 UTC (10:29 am local time), a Mw 7.4 earthquake was recorded with epicenter 23 km south of La Crucecita, Oaxaca, Mexico. According to data from the SSN, the coordinates of the epicenter are 15.784° N latitude and 96.120° W longitude, and the focal depth is 22.6 km; this earthquake is located ca. 240 km NW of the September 8, 2017 earthquake epicenter (Fig. 1).

The focal mechanism of the event (focal plane 1: strike = 266.8, dip = 17.2, rake = 60.5; focal plane 2: strike = 117.4, dip = 75.0, rake = 98.7) indicates a reverse kinematic, which a maximum slip of 3.19 m (*Servicio Sismológico Nacional*, 2020). Even if an exact relationship between the two earthquakes is not known, Guo et al. (2021), suggest that the seismic sequence started with the September 8, 2017 earthquake increased stress in the area of the June 23, 2020 earthquake, thus promoting the rupture. Miyazawa and Santoyo (2021) suggest that the September 8, 2017 earthquake could have caused changes in both dynamic and static stress. According to Guo et al. (2021), it is unlikely that the coseismic slip of the Tehuantepec earthquake was the direct cause of the 2020 Crucecita earthquake, since the Coulomb stress change was only ~0:03 bar; and the most important contribution to the occurrence of the La Crucecita earthquake was the postseismic afterslip of the 2017 Tehuantepec earthquake.

The earthquake was felt in the center and south of Mexico and in several Guatemala cities. Among the effects that the seismic event produced, damage to infrastructure has been reported both in the area near the epicenter and in 36 buildings in Mexico City (600 km away from the epicenter). According to the government report of the State of Oaxaca, as of June 24 (La Jornada Newspaper, 2020), 10 fatalities are reported, more than 2000 homes

affected in 85 municipalities, 4 archaeological zones damaged, 15 health centers affected. Earthquake environmental effects are reported, among the most outstanding, landslides, rock falls, liquefaction. Damage is also reported in Chiapas, Michoacán and Mexico City. Until January 31, there have been 15,776 aftershocks, the largest being of magnitude 5.7 on July 23, 2020 (SSN, website).

## 4. Methods

The methodological workflow that we follow in the current research is shown in Fig. 2. In the following, we describe the different steps starting from EEEs documentation and then moving to ESI-2007 intensity assignment and the analysis of the obtained macroseismic fields.

### 4.1. Documentation of earthquake environmental effects (EEEs)

For the September 8, 2017 earthquake, EEEs data collection was carried out in the field, during the first week following the event. We recorded the position using a commercial GPS and we collected photographic documentation and site description for each EEE. The data were checked by interviewing local people, to ascertain the coseismic origin of the effects. On the contrary, the data collection of EEEs generated by the earthquake of June 23, 2020 had been carried out remotely; the event occurred during the active stage of the COVID-19 pandemic and given the restrictions it was not possible to travel to the affected area.

The compilation of published data for both events was mainly done by means of scientific literature review (e.g., Chen et al., 2018; Guo et al., 2021; Gusman et al., 2018; Jiménez, 2018; Melgar et al., 2018; 2020; Ramírez-Herrera et al., 2018; Ramírez-Herrera et al., 2020; Sahakian et al., 2018; SMN, 2017; 2020; *Servicio Sismológico Nacional*, 2017; 2020; Solano et al., 2020; USGS, 2017; 2020; Velasco et al., 2020; Ye et al., 2017), newspaper (e.g., La Jornada Newspaper, 2020; El Imparcial Newspaper, 2017, 2020; Diario Marca, 2020) and online articles search, interviews, photographs, visual inspection of remote sensing imagery, and reports. Data were retained for subsequent analysis only if the geolocation is known and the reliability of the source can be assessed with objective information. The information is compared and complemented with data generated by institutions such *as Universidad Nacional Autónoma de Mexico* (UNAM), *Servicio Sismológico Nacional* (SSN), *Servicio Geológico Nacional* (SGN), remote sensing imagery and instrumental seismology data.

Following the 2020 event, we compiled an inventory of earthquake-triggered landslides by using high spatial resolution imagery (Planetscope, 3m of ground resolution). Landslides were mapped using a GIS software, by visual inspection of pre- and post-earthquake images (images captured between 16 June 2020 and 1 July 2020). In some instances, the reactivation of pre-existing landslides was documented. We marked the re-triggered slope movements by identifying the contours of the landslides before and after the earthquake. We marked each landslide from the source, identifying individual landslides before they coalesce in the toe (Tanyas et al., 2019). Several mechanisms, beside the mainshock, can trigger landslides (e.g., aftershocks, rainfall); since post-earthquake imagery was acquired no more than one week after the event, the timing of the occurrence of landslides is narrowly bracketed and suggests that most of the landslides are related to the mainshock. Due to the presence of newly formed and reactivated landslides, semi-automated and automated techniques of mapping (Sridharan et al., 2020) have not been used here, because visual interpretation, even if time-consuming, is better in mapping re-triggered landslides.

### 4.2. ESI-2007 evaluation

A detailed description of each EEE is made, taking into consideration the lithological, stratigraphic, hydrogeological and local geomorphological context, as well as size or volume of the material involved. Then, each effect is classified into primary or secondary effects; the former is directly related to the energy released by the seismogenic source and its surface expression, whereas the latter mainly depend on the local characteristics and conditions (Michetti et al., 2007; Audemard et al., 2015; Serva et al., 2016). An ESI-2007 value is assigned to each place where a single EEE of a specific type is observed (Serva et al. 2016). The supporting information includes photographs and a shapefile with the location of the sites. For landslides mapped from satellite images, we measured the area of each individual feature and we obtained the volume adopting published scaling relations (Larsen et al., 2010). We then assigned the ESI-2007 intensity based on the volume of the landslides.

### 4.3. ESI-2007 Macroseismic Field

The construction of the ESI-2007 macroseismic field had been carried out by using all the EEEs that occurred in a locality for assessing intensity data points (IDPs). The IDPs thus derive from a synthesis of multiple observations in homogeneous areas (Serva et al., 2016). Then, macroseismic fields are built based on the visual interpolation of the IDPs and with

manually drawn isoseismals. The spatial distribution of IDPs, and related intensity values was considered and a digital elevation model used as a basemap aided isoseismal drawing.

Finally, we analyze the attenuation of the ESI-2007 with distance, using the same approach developed by Chunga et al. (2018) for the Mw 7.9, Pedernales 2016 subduction event in Ecuador. We converted the macroseismic ESI-2007 field into a regular grid of 5 km resolution and calculated the median of distance for each intensity class. In order to draw broader conclusions on the intensity attenuation along subduction zones, we collected all the subduction zone earthquakes for which an ESI-2007 macroseismic field is available (Table 1). We then computed the ESI-2007 attenuation with epicentral distance and compared the different events.

We compared the ESI-2007 isoseismals maps obtained for the September 8, 2017 and June 23, 2020, earthquakes, investigating the total area affected by each earthquake and the spatial distribution of the macroseismic fields.

### 4.4. "Did You Feel It?" (DYFI) data

The DYFI system collects information from people who experience an earthquake and compiles an online form on the USGS or the *Universidad Autónoma de Nuevo León*, website. Data is gathered and made available in the form of maps, plots or raw data; these products are created within minutes of strong earthquakes and constantly updated as additional data are received. We classified data, as spatially grouped according to the postal code. The intensity of these aggregated data is expressed in terms of Community Decimal Intensity (CDI; Wald et al., 2011). Finally, we plot DYFI data and compare them with ESI-2007 values.

## 5. Results: environmental effects and intensity assessed using the ESI-2007 scale and DYFI data

In the following, we summarize the main characteristics and the spatial distribution of EEEs triggered by the two earthquakes considered in the present study. In the supplementary material (EEE_2017_2020), we provide a detailed description for each site and an intensity estimate in terms of ESI-2007 scale. Coseismic effects include either primary (permanent ground deformation, i.e., coastal subsidence or uplift) and secondary (liquefaction, cracking, slope movements) effects (Fig. 3).

### 5.1. The September 8, 2017 Gulf of Tehuantepec earthquake

During the first week after the September 8, 2017 earthquake, we surveyed the epicentral area mapping the environmental effects at 47 locations. We supplemented the database with published information, assigning ESI-2007 intensities to a total of 54 localities with values ranging between V and X degree (Figs. 4 and 5). Table 2 summarizes the number of documented IDPs for each type of EEE, the minimum and maximum distance and the ESI-2007 range. A description of each surveyed site is provided in the supplementary material (EEE_2017_2020).

Due to the offshore location of the epicenter, permanent ground displacement is only recorded in the far-field area, more than 150 km from the epicenter. Coseismic subsidence reached values of 0.9 m at Salina Cruz and Playa Vicente in Juchitán Oaxaca (Fig. 4), consistent with I = X ESI-2007. These values were documented by observing and measuring the level of subsidence and/or flooding of houses and buildings in the coastal zone and on the shore of lagoons. Field measurements are higher than GPS-derived measures, but still in the same order of magnitude (e.g., 54 cm of subsidence observed by GPS at Salina Cruz; Ye et al., 2017; Jiménez, 2018). The same discrepancy was documented for the 2016 Pedernales (Ecuador) earthquake (Chunga et al., 2018), possibly related to afterslip or the occurrence of strong aftershocks.

Among secondary effects, we documented slope movements, ground cracks, hydrological anomalies, liquefaction and tsunami effects (Fig. 5). We assigned ESI-2007 values following the guidelines of Michetti et al. (2007) and Serva et al. (2016). Slope movements were documented at 18 sites, at distances up to almost 500 km from the epicenter. The slope movements affected soils and the shallow sediments; rockfalls were documented as well. The intensity is assessed based on the volume of mobilized material, which allows to assign ESI-2007 values between V and IX. The maximum value for landslide features, I = IX ESI-2007, is given to sites where landslides with volumes up to $10^5$-$10^6$ $m^3$ have been observed. Significant ground cracks were observed at 7 IDPs, 200-500 km from the epicenter, with intensity ranging between VI and VIII. Fracture width and throw locally reached several decimeters (maximum throw: 70 cm). Individual cracks were usually of metric length, but in some cases zones up to a few hundred of meters long were affected. Liquefaction and lateral spreading were documented at 6 IDPs in a wide range of intensity (VI-IX). In the most severe cases (e.g., sites A and B in Fig. 6a), lateral spreading affected the soil for a length of hundreds of meters, with fractures showing metric aperture aligned with local water courses; I = VIII ESI-2007 was assigned to these IDPs.

Hydrogeological anomalies were documented at only 2 sites (C and D in Fig. 6a), where water turbidity and variation in discharge have been reported.

The Tehuantapec earthquake generated a tsunami recorded at numerous tide gauges along the Pacific Coast. Tsunamis are rare for normal fault ruptures with focal depths of ca. 50 km (SMN, 2017; Chen et al., 2018; Gusman et al., 2018; Ramírez-Herrera et al., 2018; Melgar et al., 2018). The maximum wave amplitude reached 3.42 m at Puerto Chiapas (site E in Fig. 6a, 181 km from the epicenter), consistent with I = IX ESI-2007. We documented wave height from tide gauge records, the run-up along the coast and damage to beaches and coastal vegetation at a total of 19 IDPs. We assigned ESI-2007 in the range between V and IX. An inundation distance of 190 m was documented at Puerto Arista (site F in Fig. 6a; Ramírez-Herrera et al., 2018).

Figure 6a shows the spatial distribution of documented EEEs according to their ESI-2007 value. IDPs are located along most of the Pacific coast of Mexico, and several observations were made inland, up to over 200 km from the Pacific coast. The total area with documented EEEs is over 200,000 $km^2$, a value which is out of scale with respect to the ESI-2007 scale guidelines (Michetti et al., 2007); this point will be further discussed in the relevant section.

ESI-2007 isoseismals are only drawn on land, since they are not traceable offshore (Fig. 6). The X degree isoseismal is elongated according to the strike of the seismogenic source and encompasses an area more than 800 km long. The elongation of the isoseismals reflects the fact that EEEs constraining the highest degrees (X and IX) mainly refer to permanent ground deformation and tsunami effects. These effects may be observed at individual points, but, indeed, permanent ground deformation affects a wide region, depending on the characteristics of the seismogenic source (kinematic, fault length and width, dip).

Some field surveys were performed to assess damage on buildings and infrastructures (e.g., Pozos-Estrada et al., 2019; Fuentes et al., 2021; Godínez-Domínguez et al., 2021). The only intensity maps covering the entire affected area derive from online questionnaires and are among the products routinely provided by the SSN and by USGS in the near real-time following strong earthquakes. Figure 7a shows the intensity derived from online questionnaires (DYFI data); it must be recalled that data are spatially aggregated and expressed in terms of CDI (Wald et al., 2011). The map includes 338 points, with a maximum intensity of 9,1 CDI. Data are spread in a wide region, up to 2500 km from the epicenter. In contrast, ESI-2007 data reach those distances only for tsunami observations. Other EEEs

have been documented at a maximum distance of 500 km from the epicenter. The distribution of DYFI data reflects population density: for instance, some clusters of points are present close to the urban conurbation of Mexico City and Guatemala City. DYFI data also include few points with low reliability, such the IDPs with CDI higher than 8 at more than 1000 km from the epicenter (Fig. 7a).

Similar to ESI-2007 intensities, CDI highest values concentrate along the coast and are elongated in a ca. NW-SE direction, matching the strike of the seismogenic source. Some points with CDI in the 6,01-7,00 class are located along the Caribbean coast and in Mexico City, ca. 400 and 700 km from the epicenter, respectively. Mexico City particularly suffers from amplification effects, due to the nature of its subsoil (Singh et al., 2018). Some of the anomalously high intensities recorded in the far field, both in terms of ESI-2007 and CDI, can be explained by amplification phenomena, due to the presence of thick sedimentary sequences (e.g., Lira & Nuñez, 2019; Moreno-Ceballo et al., 2019; Godinez-Dominguez et al., 2021) or topographic effects.

**5.2. The June 23, 2020 La Crucecita earthquake**

We documented EEEs at 125 sites (Figs. 6b, 8, 9): 47 are derived from rapid response field surveys undertaken by Ramirez-Herrera et al. (2020), 27 from a report from Universidad del Mar (Solano et al., 2020), and 51 points come from our original research on websites and social media platforms. The location of the EEEs is presented in Fig. 6b, c, showing that most of them are along a ca. 80 km long stretch of the Pacific coastline.

The epicenter lies inland, ca. 5 km from the coastline. Permanent ground deformation was documented in the epicentral region at 50 IDPs, with tectonic uplift (Fig. 8), reaching 0.8 m (Ramirez-Herrera et al., 2020), consistent with intensity = X ESI-2007. The 2020 La Crucecita earthquake generated secondary effects such as ground cracks, hydrological changes, liquefaction and tsunami (Fig. 9). Just as for the 2017 Tehuantepec earthquake, we assigned ESI-2007 values following the guidelines of Michetti et al. (2007) and Serva et al. (2016).

Slope movements were documented at 42 sites, located between 3 and 112 km from the epicenter; the volume of mobilized material allows to assign ESI-2007 values between V and VIII. Significant landslides with volumes estimated around $10^4$ $m^3$ completely blocked major roads up to ca. 100 km from the epicenter and were assigned I = VIII ESI-2007 (e.g.,

site G in Fig. 6b: km 188 of Oaxaca – Tehuantepec highway; site H in Fig. 6b: Totolapan – Oaxaca highway).

Ground cracks were recorded at 19 IDPs, in the ESI-2007 range VI-X; in the worst-affected places (sites I and J in Fig. 6c), cracks were ca. 500 m long and had metric width. Liquefaction was documented at 4 IDPs, where we assigned intensities between VI and VIII and no more than 25 km from the epicenter (e.g., sites K and L in Fig. 6c); sand volcanoes had a maximum diameter of ca. 1 meter.

Tsunami was observed at 9 IDPs, located at 2-50 km from the epicenter; maximum amplitude in the order of 1.5 m allows to assign maximum intensity = VIII ESI-2007 (e.g., site M in Fig. 6b, tide gauge at Salina Cruz, 107 km from the epicenter).

Ground cracks and landslides were documented either along the coastline and inland. However, observations points are biased because they are preferentially located along infrastructures: the local news sources (see “website resources” in the reference list) were prone to document damage along the road network or in the proximity of inhabited areas, while EEEs in remote areas easily went unnoticed. In order to have an independent and unbiased source of information, we mapped slope movements from satellite imagery; we focused on a ca. 800 $km^2$ area (Fig. 6), where 304 landslides were mapped. The biggest landslides have a volume in the order of $10^4$ to $10^5$ $m^3$, corresponding to ESI-2007 VIII. Several landslides were already present before the earthquake (see Fig. 10), and we were careful in mapping only re-triggered or newly generated movements. The total area affected by secondary effects is of ca. 14,000 $km^2$, suggesting an XI ESI-2007.

For the 2020 earthquake, it was possible to draw only the X, IX and VIII ESI-2007 isoseismal lines; the one corresponding to X and IX ESI-2007 occupy a narrow band along the coast, while the VIII isoseismal include a much wider region inland (Fig. 6).

Fig. 7b shows the intensity derived from online questionnaires (DYFI data); the map includes 185 points, with a maximum intensity of 7,7 CDI and distances up to ca. 2500 km from the epicenter (as a comparison, the furthest ESI-2007 point is located 130 km from the epicenter). The maximum CDI intensity is much lower than the ESI-2007 epicentral intensity, assessed at X. As for the 2017 event, a cluster of DYFI data points is located close to Mexico City.

## 6. Discussion

### 6.1. Surveying strategies: field vs remote sensing methodologies

The 2017 and 2020 earthquakes were analyzed using completely different methodologies: in the first case, a typical fieldwork study was undertaken, involving mapping and *in situ* measurements. The 2020 earthquake instead occurred during the COVID-19 pandemic, preventing detailed fieldwork and forcing us to adapt and adopt different strategies. No fieldwork has been performed and data come from remote sources only (scientific literature, satellite imagery, social media and online sources). Landslide mapping from satellite imagery proved particularly useful in remote areas, where documentation from other sources was poor. Mapping from satellite images allows to investigate the territory in an unbiased way and to map landslides with areas as low as ca. 100 $m^2$, corresponding to ESI-2007 VI. On the contrary, eyewitness reports are highly clustered along the communication network and much smaller landslides were documented only if they are proximal to the road network or other infrastructures. Data collected from satellite images and eyewitness reports are indeed complementary.

The collection of data from remote sources poses some challenges. The location of the documented EEEs, in particular from local newspapers or websites, may be less accurate than what can be achieved during fieldwork and using a GPS. We tackled this issue by retaining only information where the locality is identifiable; location uncertainties in the order of a few kilometers do not heavily affect our results due to the scale of our analysis (see for instance the scale of Fig. 6). Intensity assignment may be difficult if available data are only a few photographs and anon-technical description.

### 6.2. ESI-2007 intensity assignment

The metrics used to assign an ESI-2007 intensity depend on the type of EEEs at each locality, such as amount of ground displacement, length and width of ground cracks and volume of slope movement. The ESI-2007 intensity can be assigned also from the dimension of the area affected by secondary effects (Michetti et al., 2007; Serva et al., 2016). In Table 2 we list the maximum observed values for the main types of EEEs following the 2017 and 2020 earthquakes, namely permanent ground deformation, tsunamis and landslides. Individual EEEs consistently point toward a maximum intensity of X ESI-2007. On the contrary, the ESI-2007 value derived from the total area affected by secondary EEEs is much higher. The same observation was made following the 2016 Pedernales (Ecuador) earthquake (Chunga et al., 2018).

Such a discrepancy may have different possible and concurrent explanations:

a) regions prone to coseismic effects located in the far-field significantly expand the total area affected by secondary EEEs (e.g., Chunga et al., 2018); isolated data located far from the epicenter strongly affect the values of total affected area, if it is measured by drawing a polygon encompassing all the documented EEEs;

b) the total area affected by secondary effects might be influenced by the focal depth, that in subduction earthquakes is larger than for shallow crustal events, leading to longer and more circular isoseismals; a notable example of large affected area is given by the 1755 earthquake; secondary effects occurred in the whole Iberian Peninsula and hydrological and hydrogeological anomalies were recorded as far as Central Europe (Silva et al., 2017);

c) the values provided in the ESI-2007 guidelines for assessing intensity from the total affected area are underestimated; it must be noted that these values are empirical and were provided when the ESI-2007 scale was first released (Michetti et al., 2007).

The values provided in the ESI-2007 guidelines do not consider the seismotectonic setting and thus may be valid for shallow crustal earthquakes, but not for events in subduction zones. In any case, the location and kinematics of the seismogenic source matters: as reported by Van Daele et al. (2019), higher-frequency accelerations from intraplate earthquakes would be hardly attenuated in rocks whereas lower-frequency accelerations from megathrust earthquakes would be amplified in soft sediments.

### 6.3. Intensity attenuation and comparison between interface and intraslab earthquakes

The different behavior between interface (thrust focal mechanism) and intraslab (normal focal mechanism) earthquakes in subduction zones has been investigated either through intensity (e.g., Chavez & Castro, 1988) or ground motion (e.g., Furumura & Singh, 2002; Atkinson & Boore, 2003; Sahakian et al., 2018) attenuations with distance from the hypocenter or seismogenic source.

Beside the two events analyzed in the present paper, ESI-2007 macroseismic fields are available for two other subduction earthquakes (Table 1), namely the 2011 Mw 9.0 Tohoku (Japan; Sanchez & Maldonado, 2016) and 2016 Mw 7.8 Pedernales (Ecuador; Chunga et al., 2018) earthquakes.

Figure 11a shows the attenuation of ESI-2007 intensity from the hypocenter for all the available subduction zone earthquakes. Symbols are the median distance for each intensity class, while lines are least-square fittings. The 2017 Tehuantepec event is the only intraslab earthquake, so further case histories are needed to derive robust comparisons. Nevertheless, some preliminary interpretations can be drawn from Figure 11a; at a given distance, the intensity of the 2017 Tehuantepec event is higher than the other 3 earthquakes, and its attenuation is less steep. The ESI-2007 scale is known to perform better in the near-field rather than in the far-field (e.g., Papanikolaou et al., 2009; Chunga et al., 2018), so the extrapolation at low degrees should be carefully considered. Moreover, another source of uncertainty is related to the availability of incomplete macroseismic fields, due to offshore regions. The attenuation for the 2017 earthquake is marked as a dotted line, to underline its preliminary character. A comparison with other intraslab earthquakes will provide more insights on the ESI attenuation in such a setting.

We also plot the only Intensity Prediction Equation (IPE) available for the ESI-2007 scale, developed from shallow crustal, normal faulting earthquakes in the Italian Apennines (Ferrario et al., 2020; Fig. 11a). Since the original IPE is derived in terms of epicentral distance, we calculated it by assuming a focal depth of 10 km, which is a reliable value for the Italian Apennines, and an epicentral intensity of IX ESI-2007.

In figure 11c we show the relation among ESI-2007 epicentral intensity and moment magnitude by comparing subduction zone earthquakes with events in the Mediterranean region (Papanikolaou & Melaki, 2017). For a given ESI-2007 intensity, subduction events show a much higher magnitude, thus pointing to the role of the seismotectonic setting in driving such empirical relations. We also examine the pattern of MM intensity attenuation for different seismotectonic settings in Mexico, assuming a Ms 7.0 earthquake: shallow crustal events in the Trans-Mexican Volcanic Belt, intraslab and interface earthquakes (Chavez & Castro, 1988; Fig. 11b). Intraslab earthquakes show the highest intensity up to ca. 250 km, where the intensity due to interface events becomes higher. Observed ground motions for the 2017 Tehuantapec event are higher than expected from available prediction equations, possibly driven by subduction zone geometry (Sahakian et al., 2018).

We remark that IPEs for shallow crustal earthquakes are widely developed, whereas subduction zones have been the focus of much more limited research (Cua et al., 2010). IPEs for the ESI-2007 scale are still in their infancy and hold a great potential for future developments. For instance, the attenuations in Figure 11a are based on hypocentral

distance, which can be a gross simplification in case of strong events, where the point-source assumption is no longer valid. Future work should consider instead distance from the fault rupture.

## 7. Conclusions

From the analysis of the data discussed above, the following main conclusions can be drawn.

- We collected Earthquake Environmental Effects for the 2017 Tehuantapec and 2020 La Crucecita, Oaxaca earthquakes, which represent intraslab and interface settings, respectively; primary effects include coastal subsidence and uplift, while secondary effects include open cracks, landslides, rock fall, liquefaction and lateral spreading and tsunami generated by both events.
- We assess local ESI-2007 values at 54 and 123 sites, for the two study earthquakes; the epicentral intensity is estimated at X for both events using the ESI-2007 scale; we draw isoseismals and analyze the attenuation of ESI-2007 intensity with distance; a good consistency with other subduction events is found, testifying that the ESI-2007 scale is a reliable tool, since it behaves consistently among different events.
- We compare ESI-2007 intensities with estimates deriving from online questionnaires (DYFI data), showing that they provide complementary information; the ESI-2007 scale has been successfully integrated with traditional, damage-based scales; we envisage that a similar effort can be made using DYFI data, which will result in a more comprehensive image of the overall earthquake effects.
- Seismic hazard along the Mexican coast is dominated by megathrust events, but a significant hazard may derive from intraslab events; at a given distance, intraslab events may generate higher intensity and ground motion when compared to interface earthquakes, pointing to the need of a proper evaluation of the seismogenic setting in seismic risk assessment.
- The September 8, 2017, Tehuantepec earthquake is the first offshore intraslab earthquake studied using the ESI-2007 scale; this work is expected to mark the beginning of research in which the analysis of EEEs in subduction zones in Mexico, and possibly worldwide, will be systematically included in the evaluation of the size and intensity of an earthquake.

## Author contributions

**Velázquez-Bucio M.M.**: Investigation, Formal analysis, Writing – original draft, contribution in data acquisition; **Ferrario M.F.**: Investigation, Formal analysis, Methodology, Writing – original draft; **Muccignato E.**: Visualization, contribution in data acquisition; **Porfido S.**: Conceptualization, Methodology, Supervision; **Sridharan A.**: Formal analysis, Methodology; **Chunga K.**: Methodology; Formal analysis; **Livio F.**: Formal analysis, Writing – review & editing; **Gopalan S.**: Formal analysis, Methodology; **Michetti A.M.**: Conceptualization, Investigation, Methodology, Supervision, Writing – review & editing. All authors have read and agreed to the published version of the manuscript.

## Data availability

Data in this article are openly available. Historical seismicity is from Servicio Sismológico Nacional (SSN), http://www2.ssn.unam.mx:8080/catalogo/. All Servicio Sismológico Nacional data can be obtained at www.ssn.unam.mx

Tide gauge data are provided by the Servicio Mareográfico Nacional (SMN), http://www.mareografico.unam.mx/portal/. DYFI data can be downloaded from the USGS website at the following links:

https://earthquake.usgs.gov/earthquakes/eventpage/us2000ahv0/executive
https://earthquake.usgs.gov/earthquakes/eventpage/us6000ah9t/executive.

The supplementary material for this article provides a detailed description and figure for each site with an intensity estimate in terms of ESI-2007 scale. It also provides shapefiles with the location of the EEE's and the isoseismals corresponding to the September 8, 2017, and June 23, 2020, earthquakes in terms of the ESI-2007 scale.

## Declaration of competing interest

The authors declare that they have no known competing financial interests or personal relationships that could have appeared to influence the work reported in this paper.

## Acknowledgements

Dr. Víctor H. Garduño-Monroy helped with scientific discussion; his untimely death has left a great void, and this work is dedicated to his memory. We are grateful to geologist Sergio Nájera for his help in the fieldwork. Thanks to Mr. A. Gerardo Ramírez Díaz, of the Topos Azteca International Rescue Brigade (B.I.R.T.A.), Oaxaca and to the Oaxaca State Police, for their support and accompaniment during the collection of the effects of the Tehuantepec earthquake, 2017. Thanks to the SSN, SMN, UNAM, UMAR and the people who published data on the effects of the 2017 Tehuantepec and 2020 La Crucecita earthquakes, which we have used to carry out this work.

## References

Atkinson, G.M., Boore, D.M., 2003. Empirical ground-motion relations for subduction-zone earthquakes and their application to Cascadia and other regions, Bull. Seismol. Soc. Am. 93, no. 4, 1703–1729.

Audemard, F., Azuma, T., Baiocco, F., Baize, S., Blumetti, A.M., Brustia, E., Clague, J., Comerci, V., Esposito, E., Guerrieri, L., Gurpinar A., Grützner C., Jin K., Kim Y.S., Kopsachilis V., Lucarini M., McCalpin J., Michetti A.M., Mohammadioun B., Morner N.A., Okumura K., Ota Y., Papathanassiou G., Pavlides S., Pérez López R., Porfido S.,Reicherter K., Rodríguez Pascua M.A., Roghozin E., Scaramella A., Serva L., Silva P.G., Sintubin M., Tatevosssian R., Vittori E., 2015. Earthquake Environmental Effects for Seismic Hazard Assessment: The ESI Intensity Scale and the EEE Catalogue; ISPRA: Rome, Italy, 2015, Volume 97, ISBN 978-88-9311-007-5.

Caccavale, M., Sacchi, M., Spiga, E., Porfido, S., 2019. The 1976 Guatemala Earthquake: ESI Scale and Probabilistic/Deterministic Seismic Hazard Analysis Approaches, Geosciences, 9, 403, doi:10.3390/geosciences9090403

Chavez M., Castro, R., 1988. Attenuation of Modified Mercalli intensity with distance in Mexico. Bull. Seismol. Soc. Am., 78, 6, 1875-1884.

Chen K., Feng, W., Liu, Z., Song, Y.T., 2018. Mw 8.1 Tehuantepec Earthquake: Deep Slip and Rupture Directivity Enhance Ground Shaking but Weaken the Tsunami, Seismological Research Letters, Early Edition. doi: 10.1785/0220170277

Chunga, K., Livio, F., Mulas, M., Ochoa-Cornejo, F., Besenzon, D., Ferrario, M.F., Michetti, A.M., 2018. Earthquake ground effects and intensity of the 16 April 2016 Mw 7.8 Pedernales, Ecuador, earthquake: Implications for the source characterization of large subduction earthquakes, Bull. Seismal. Soc. Am. 108, 6, 3384-3397, doi: 10.l 785/0120180051

Cua G., Wald, D.J., Allen, T.I., Garcia, D., Worden, C. B., Gerstenberger, M., Lin, K., Marano, K., 2010. “Best Practices” for Using Macroseismic Intensity and Ground Motion Intensity Conversion Equations for Hazard and Loss Models in GEM1. GEM Technical Report 2010-4, GEM Foundation, Pavia, Italy.

DeMets, C., Gordon, R.G., Argus D.F., 2010. Geologically current plate motions, Geophys. J. Int. 181, no. 1, 1–80.

Ferrario, M.F., Livio, F., Capizzano, S.S., Michetti, A.M., 2020. Developing the first Intensity Prediction Equation based on the Environmental Scale Intensity: A case study from strong normal-faulting earthquakes in the Italian Apennines. Seismological Research Letters, 91(5), 2611-2623.

Fuentes D.D., Baquedano Julià P.A., D'Amato M., Laterza M., 2021. Preliminary seismic damage assessment of Mexican churches after September 2017 earthquakes. International Journal of Architectural Heritage, 15(4), 505-525.

Furumura T., Singh, S. K., 2002. Regional Wave Propagation from Mexican Subduction Zone Earthquakes: The Attenuation Functions for Interplate and Inslab Events. Bull. Seismol. Soc. Am., 92, 6, 2110-2125.

Godínez-Domínguez E.A., Tena-Colunga A., Pérez-Rocha L.E., Archundia-Aranda H.I., Gómez-Bernal A., Ruiz-Torres R.P., Escamilla-Cruz J.L., 2021. The September 7, 2017 Tehuantepec, Mexico, earthquake: Damage assessment in masonry structures for housing. International Journal of Disaster Risk Reduction, 56, 102123.

Guo, R., Yang, H., Zhu, Y., Zheng, Y., Xu, J., Zhang, L., An, C., 2021. Narrow Rupture of the 2020 Mw 7.4 La Crucecita, Mexico, Earthquake, Seismol. Res. Lett. XX, 1–9, doi: 10.1785/0220200328

Gusman, A.R., Mulia, I.E., Satake, K., 2018. Optimum sea surface displacement and fault slip distribution of the 2017 Tehuantepec earthquake (Mw 8.2) in Mexico estimated from tsunami waveforms. Geophysical Research Letters, 45, 646–653, https://doi.org/10.1002/2017GL076070

Huayong N., Hua, G., Yanchao, G., Blumetti, A.M., Comerci, V., Di Manna, P., Guerrieri, L., Vittori, E., 2019. Comparison of Earthquake Environmental Effects and ESI intensities for recent seismic events in different tectonic settings: Sichuan (SW China) and Central Apennines (Italy), Engineering Geology, 258, (105149), DOI: 10.1016/j.enggeo.2019.105149

Jiménez, C., 2018. Seismic Source Characteristics of the Intraslab 2017 Chiapas-Mexico Earthquake (Mw8.2), Physics of the Earth and Planetary Interiors, doi: Larsen, I. J., Montgomery, D. R., Korup, O., 2010 Landslide erosion caused by hillslope material. Nature Geosci. 3, 247-251.

King, T.R., Quigley M., Clark D., 2019. Surface-Rupturing Historical Earthquakes in Australia and Their Environmental Effects: New Insights from Re-Analyses of Observational Data. Geosciences, 9, 408, https://doi.org/10.3390/geosciences9100408

Lira, J., & Nuñez, M., 2019. Subsidence and Morphologic Variations in Mexico City Generated by the Earthquakes of September 2017. Geofísica internacional, 58(3), 211-227.

Melgar D., Ruíz-Ángulo, A., Soliman, G.E., Manea, M., Manea, V.C., Xu, X., Ramirez-Herrera, M.T., Zavala-Hidalgo, J., Geng, J., Corona, N., Pérez-Campos, X., Cabral-Cano, E., Ramirez-Guzman, L., 2018. Deep embrittlement and complete rupture of the lithosphere during the Mw 8.2 Tehuantepec earthquake. Nature Geoscience Articles. https://doi.org/10.1038/s41561-018-0229-y

Melgar D., Ruiz-Angulo, A., Pérez-Campos, X., Crowell, B.W., Xu, X., Cabral-Cano, E., Brudzinsky, M.R., Rodríguez-Abreu, R., 2020. Energetic Rupture and Tsunamigenesis during the 2020 Mw 7.4 La Crucecita, Mexico Earthquake, Seimol. Res. Lett. XX, 1-11, doi: 10.1785/0220200272.

Michetti A.M., Esposito, E., Guerrieri, L., Porfido, S., Serva, L., Tatevossian, R., Vittori, E., Audemard, F., Azuma, T., Clague, J., Comerci, V., Gürpinar, A., McCalpin, J., Mohammadioun, B.,

Mörner, N.A., Ota, Y., Roghozin, E., 2007. Environmental Seismic Intensity Scale 2007 - ESI 2007. Memorie Descrittive della Carta Geologica d'Italia, 74, 7-54, Servizio Geologico d'Italia – Dipartimento Difesa del Suolo, APAT, Roma, Italy, http://www.isprambiente.gov.it/en/publications/technical-periodicals/descriptive-memories-of-the-geological-map-of/intensity-scale-esi-2007?set_language=en

Moreno Ceballo, R., González Herrera, R., Paz Tenorio, J. A., Aguilar Carboney, J. A., & Del Carpio Penagos, C. U., 2019. Effects of Sediment Thickness upon Seismic Amplification in the Urban Area of Chiapa de Corzo, Chiapas, Mexico. Earth Sciences Research Journal, 23(2), 111-117.

Papanikolaou, I.D., Papanikolaou, D.I., Lekkas, E.L., 2009. Advances and limitations of the Environmental Seismic Intensity scale (ESI 2007) regarding near-field and far-field effects from recent earthquakes in Greece: Implications for the seismic hazard assessment, Geol. Soc. Spec. Publ. 316, 11–30.

Papanikolaou, I.D., 2011. Uncertainty in intensity assignment and attenuation relationships: How seismic hazard maps can benefit from the implementation of the Environmental Seismic Intensity scale (ESI 2007), Quaternary International, 242, 42-51, doi: 10.1016/j.quaint.2011.03.058.

Porfido, S., Alessio, G., Gaudiosi, G., Nappi, R., 2020. New Perspectives in the Definition/Evaluation of Seismic Hazard through Analysis of the Environmental Effects Induced by Earthquakes, Geosciences, 10, 58, doi:10.3390/geosciences10020058.

Ramírez-Herrera MT., Corona, N., Ruiz-Angulo, A., Melgar, D., Zavala-Hidalgo, J., 2018. The 8 September 2017 Tsunami Triggered by the M w 8.2 Intraplate Earthquake, Chiapas, Mexico. Pure and Applied Geophysics, 175-25-34. DOI 10.1007/s00024-017-1765-x

Ramírez-Herrera, M.-T., Romero, D., Corona, N., Nava, H., Torija, H., Hernández Maguey, F., 2020. The 23 June 2020 Mw 7.4 La Crucecita, Oaxaca, Mexico Earthquake and Tsunami: A Rapid Response Field Survey during COVID-19 Crisis, Seismol. Res. Lett. XX, 1–12, doi: 10.1785/0220200263

Sahakian, V.J., Melgar, D., Quintanar, L., Ramírez-Guzmán, L., Pérez-Campos, X., Baltay, A., 2018. Ground Motions from the 7 and 19 September 2017 Tehuantepec and Puebla-Morelos, Mexico, Earthquakes. Bull. Seismol. Soc. Am., doi: 10.1785/0120180108

Sanchez, J.J., & Maldonado, R.F., 2016. Application of the ESI 2007 scale to two large earthquakes: South Island, New Zealand (2010 M w 7.1), and Tohoku, Japan (2011 M w 9.0). Bulletin of the Seismological Society of America, 106(3), 1151-1161.

Segou, M., Parsons, T., 2018. Testing earthquake links in Mexico from 1978 to the 2017 M = 8.1 Chiapas and M = 7.1 Puebla shocks. Geophysical Research Letters, 45, 708–714. https://doi.org/10.1002/2017GL076237

Serva, L., Vittori, E., Comerci, V., Esposito, E., Guerrieri, L., Michetti, A.M., Mohammadioun, C., Porfido, S., Tatevossian, R.E., 2016, Earthquake Hazard and the Environmental Seismic Intensity (ESI) Scale: Pure and Applied Geophysics, 173 (5) 1479 – 1515, DOI 10.1007/s00024-015-1177-8

SMN (Servicio Mareográfico Nacional), 2017. Registro de variaciones del nivel del mar en las estaciones del Servicio Mareográfico Nacional causadas por el sismo del 7 de septiembre de 2017 al suroeste de Pijijiapan, Chiapas. Reporte del Instituto de Geofísica – UNAM.

SMN (Servicio Mareográfico Nacional), 2020. Reporte del tsunami producido por el sismo de magnitud 7.5 ocurrido el día 23 de junio. de 2020 al sureste de Crucecita, Oaxaca. Reporte del Instituto de Geofísica – UNAM.

Servicio Sismológico Nacional, 2017. Reporte Especial: Sismo de Tehuantepec (2017-09-07 23:49 Mw 8.2), IGEF-UNAM, México, available online at http://www.ssn.unam.mx/sismicidad/reportes-especiales/2017/SSNMX_rep_esp_20170907_Tehuantepec_M82.pdf

Servicio Sismológico Nacional, 2020. Reporte Especial: Sismo del 23 de Junio de 2020, Costa de Oaxaca (M 7.5), IGEF-UNAM, México, available online at http://www.ssn.unam.mx/sismicidad/reportes-especiales/2020/SSNMX_rep_esp_20200623_Oaxaca-Costa_M75.pdf.

Silva P.G., Gómez-Diego P.V., Elez J., Giner-Robles J.L., Rodríguez-Pascua M.Á., Roquero E., Martínez-Graña A., Bardají T., Bautista B., 2017. Earthquake environmental effects of the AD 1755 Lisbon-Earthquake-Tsunami in Spain. In Mudanças em Sistemas Ambientais e sua Expressão Temporal: Livro de Resumos da IX Reunião do Quaternário Ibérico (pp. 53-57). Asociación Española para el Estudio del Cuaternario.Silva, P.G., Rodríguez-Pascua M.A., Giner Robles J.L., Élez J., Pérez-López R., Davila M.B.B., 2019. Catalogue of the Geological Effects of Earthquakes in Spain Based on the ESI-07 Macroseismic Scale: A New Database for Seismic Hazard Analysis. Geosciences, 9, 334.

Singh, S.K., Astiz, L., Havzkov, J., 1981. Seismic gaps and recurrence periods of large earthquakes along the Mexican subduction zone: A reexamination, Bull. Seismol. Soc. Am., 71, 827–843.

Singh, S.K., Ordaz, M., Alcántara, L., Shapiro, N., Kostoglodov, V., Pacheco, J.F., Alcocer, S., Gutiérrez, C., Quaas, R., Mikumo, T., Ovando, E., 2000. The Oaxaca Earthquake of 30 September 1999 (Mw = 7. 5): A Normal-faulting Event in the Subducted Cocos Plate, Seismological Research Letters Vol. 71, 1, 67-78.

Singh S.K., Reinoso E., Arroyo D., Ordaz M., Cruz- Atienza V., Pérez- Campos X., Hjörleifsdóttir V., 2018. Deadly intraslab Mexico earthquake of 19 September 2017 (M w 7.1): Ground motion and damage pattern in Mexico City. Seismological Research Letters, 89(6), 2193-2203.

Solano, E.A., Zavala, T.B., Ramírez, C.E., Cervantes, A., Ortíz, M.L.J., Leyte, M.G., Hernández, B.L.M., Benítez, V.F., Ahumada, S.M.A., Illescas, E.O., Reyes, G.I., 2020. Reporte de actividades de los levantamientos en campo del sismo del 23 de junio de 2020 (M 7.4) llevado a cabo por profesores y técnicos de la UMAR campus Puerto Ángel. UMAR. Oaxaca, Mexico, 15 pp., available online at http://huatulco.umar.mx/avisos/Resumen_Efectos_del_sismo_del_23_de_junio_2020.pdf, doi: 10.13140/RG.2.2.20638.25929

Sridharan, A., AS. Ajai, R., Gopalan, S., 2020. A Novel Methodology for the Classification of Debris Scars using Discrete Wavelet Transform and Support Vector Machine. Procedia Computer Science, 171, 609-616.

Suárez, G., Albini, P., 2009. Evidence for great tsunamigenic earthquakes (M 8.6) along the Mexican subduction zone. Bull. Seismol. Soc. Am. 99 (2A), 892–896, doi: 10.1785/0120080201.

Suárez G., Santoyo, M.A., Hjorleifsdottir, V., Iglesias, A., Villafuerte, C., Cruz-Atienza, V.M., 2019. Large scale lithospheric detachment of the downgoing Cocos plate: The 8 September 2017 earthquake (Mw 8.2). Earth and Planetary Science Letters 509, 9–14, doi.org/10.1016/j.epsl.2018.12.018

Suárez, G., Ruiz-Barón, D., Chico-Hernández, C., Zúñiga, F.R., 2020. Catalog of Preinstrumental Earthquakes in Central Mexico: Epicentral and Magnitude Estimations Based on Macroseismic Data, Bull. Seismol. Soc. Am. XX, 1–16, doi: 10.1785/0120200127

Tanyaş, H, Van Westen, C.J., Allstadt. K.E., Jibson. R.W., 2019. Factors controlling landslide frequency–area distributions. Earth Surf. Process. Landforms, 44, 900–917 (2019), DOI: 10.1002/esp.4543

USGS, 2017, M 8.2 - near to the coast of Chiapas, Mexico, available online at https://earthquake.usgs.gov/earthquakes/eventpage/us2000ahv0/executive#executive.

USGS, 2020, M 7.4 - 9 km SE of Santa María Xadan, Mexico, available online at https://earthquake.usgs.gov/earthquakes/eventpage/us6000ah9t/executive.

Van Daele, M., Araya-Cornejo, C., Pille, T., Vanneste, K., Moernaut, J., Schmidt, S., Kempf, P., Meyer, I., Cisternas, M., 2019. Distinguishing intraplate from megathrust earthquakes using lacustrine turbidites. Geology, *47*(2), 127-130.

Velasco, A., A., Pérez-Campos, X., Husker, A., Karplus, M. S., Gonzalez-Huizar, H., Ayala Cortez, S., 2020, La Crucecita earthquake illustrates quake risk in México, Temblor, http://doi.org/10.32858/temblor.097

Wald, D.J., Quitoriano, V., Worden, C.B., Hopper, M., Dewey, J.W., 2011. USGS “Did You Feel It?” internet-based macroseismic intensity maps. Annals of Geophysics, 54, 6, 2011; doi: 10.4401/ag-5354.

Ye L., Lay, T., Bai, Y., Cheung, K.F., Kanamori, H., 2017. The 2017 Mw 8.2 Chiapas, Mexico, Earthquake: Energetic Slab Detachment, Geophysical Research Letters, 44, 11,824–11,832, https://doi.org/10.1002/2017GL076085

Zúñiga, F.R., Suárez, G., Figueroa-Soto Á., Mendoza A., 2017. A first-order seismotectonic regionalization for seismic hazard and risk estimation, J. Seismol. 21, 1295–1322, doi: 10.1007/s10950-017-9666-0

## Websites Resources

ADN 40, 2020. Se secan las cascadas de Agua Azul. 2017. https://www.adn40.mx/noticia/mexico/nota/2017-11-12-07-55/se-secan-las-cascadas-de-agua-azul/, last accessed, 05 05 2021.

Cracking_Guivini, 2020, https://www.facebook.com/photo?fbid=611306216437773&set=pcb.2559545640929674, last accessed 18 08 2021.

Cracking_RíoHondo, 2020,: https://www.facebook.com/Oaxacavialynoticiasalinstante/posts/2730071280646554, last accessed 27 06 2021.

Cracking_VentanillaBeach, 2020, https://www.facebook.com/YoAMOHuatulco/photos/a.1448197402161100/2580139742300188, last accessed 14 05 2021.

Diario Marca, 2020.Diario Marca, La historia de Oaxaca. Liberaron carril en carretera al Istmo tras derrumbe por sismo. 2017. https://www.diariomarca.com.mx/2020/06/liberaron-carril-en-carretera-al-istmo-tras-derrumbe-por-sismo/, last accessed, 18 08 2021.

El Imparcial Newspaper, 2017. El imparcial, El mejor diario de Oaxaca. Se abre la tierra en San Juan Ñumi, Oaxaca. http://imparcialoaxaca.mx/policiaca/58485/se-abre-la-tierra-en-san-juan-numi-oaxaca/, last accessed, 07 09 2021.

El Imparcial Newspaper, 2020. El imparcial, Del Istmo. Se desgaja cerro en Mixtequilla por sismo. https://imparcialoaxaca.mx/istmo/443580/se-desgaja-cerro-en-mixtequilla-por-sismo/, last accessed, 07 09 2021.

La Jornada Newspaper, 2014. Sobrexplotación pesquera amenaza a toda la comunidad de Playa Vicente. https://www.jornada.com.mx/2014/11/02/estados/028n1est, last accessed, 20 08 2021.

La Jornada Newspaper, 2020. Diez muertos por sismo en Oaxaca; daños en 85 municipios: Murat, https://www.jornada.com.mx/ultimas/estados/2020/06/24/siete-muertos-por-sismo-en-oaxaca-danos-en-85-municipios-murat-812.html, last accessed, 05 09 2021.

Landslide_Ozolotepec, 2020, https://www.facebook.com/2LopezIsaac/posts/1395485320656705, last accessed 07 09 2021.

Página 3, Newspaper, 2015. Periodismo humano con misión social. Playa Vicente, destino turístico preferido de juchitecos. https://pagina3.mx/2015/04/playa-vicente-destino-turistico-preferido-de-juchitecos/, last accessed, 20 08 2021.

Rockfall_Guivini, 2020, https://www.facebook.com/photo?fbid=611305826437812&set=pcb.2559545640929674, last accessed 06 09 2021.

SSN, (*Servicio Sismológico Nacional*), catalog, Catálogo de Sismos, http://www2.ssn.unam.mx:8080/catalogo/, last accessed, 09 08 2021.

SSN, (*Servicio Sismológico Nacional*), website, http://www.ssn.unam.mx/, last accessed, 29 08 2021.

Tsunami_Huatulco, 2020, https://www.facebook.com/YoAMOHuatulco/photos/a.1448197402161100/2580082382305924, last accessed 14 05 2021.

Universidad Autónoma de Nuevo León. ¿Sintió un sismo?, http://fct.uanl.mx/encuestas/sintio-un-sismo/, last accessed, 21 08 2021.

## Figure captions

Figure 1. Epicenters of the September 8, 2017 and June 23, 2020 earthquakes; inset shows the position of the study area in the plate tectonics setting of Mexico and Central America.

Figure 2. Methodological workflow followed in the present work.

Figure 3. Type of Earthquake Environmental Effects documented during the Sept. 8, 2017, Mw 8.2, Tehuantepec earthquake (green), and the June 23, 2020, Mw 7.4, La Crucecita, earthquake (brown).

Figure 4. Example of primary effects generated by the September 8, 2017 earthquake; Vicente Beach site before (a, a') and after (b) the September 8, 2017, earthquake; coastal subsidence; a (view looking north; source: La Jornada, Newspaper, 2014), a' (view looking south; source: Página 3, Newspaper, 2015), images of Vicente Beach in which it is possible to see the difference in the water level and the beach space between the small constructions (*palapas*) and the sea before the earthquake; b (view looking north; photo taken by M. Velazquez-Bucio on September 13, 2017) permanent coastal flooding due to 0.5 m coseismic tectonic subsidence at Vicente Beach, 200 km from the epicenter; I = X ESI-2007

Figure 5. Example of secondary effects generated by the September 8, 2017 earthquake. a), a') cracking in natural soil road, 40 cm wide, 143 cm depth, Salina Cruz, Oaxaca, I = VIII ESI-2007 (photos taken by M. Velazquez-Bucio on September 13, 2017); b) Landslide ca. $10^4$-$10^5$ $m^3$ in volume; landslide caused fractures up to 300 cm of width and 500 meters length in saturated soil, San Juan Ñumi, Oaxaca, (El Imparcial Newspaper, 2017), I = VIII ESI-2007; c) negative variation of water flow with consequent drainage of the source, Cascadas de Agua Azul, Chiapas, (ADN 40, 2020), I = VII ESI-2007; d), e) tectonic subsidence and cracking 6 cm wide, Vicente Beach, Juchitán, Oaxaca, I = X and VIII ESI-2007 (photos taken by M. Velazquez-Bucio on September 12, 2017); f) fractures in asphalt with vertical displacement of 15-17 cm; fractures parallel to the direction of the axis of the road of about 3 m, with 2 cm of opening, Xadani, Oaxaca, I = VIII ESI-2007 (photo taken by M. Velazquez-Bucio on September 13, 2017); g) landslide and rock fall of $10^4$ $m^3$ and fractures of 40 cm of length and 1.40 m of depth, Cañón del Sumidero, Chiapas (Velázquez-Bucio et al., 2017), I = VIII ESI-2007; h) 3,42 m high tsunami waves (Servicio Mareográfico Nacional, 2017), I = IX ESI-2007

Figure 6: a) EEEs and ESI-2007 isoseismals following the 8 September 2017 earthquake; the black rectangle is the area enlarged in b; capital letters refer to significant sites mentioned in the text. A: lateral spreading at Jaltipan de Morelos, I = VIII ESI-2007; B: lateral spreading at Acachapan y Colmena, I = VIII ESI-2007; C: hydrogeological anomaly at Cascadas de Agua Azul, I = VII ESI-2007; D: hydrogeological anomaly at Santiago Laollaga, I = VI ESI-2007; E: tsunami at Puerto Chiapas, I = IX ESI-2007; F: tsunami at Puerto Arista, I = VIII ESI-2007. b) EEEs and ESI-2007 isoseismals following the 23 June 2020

earthquake; the black rectangle is the area enlarged in c; capital letters refer to significant sites mentioned in the text. G: landslides along the Oaxaca – Tehuantepec highway, I = VIII ESI-2007; H landslides along the Totolapan – Oaxaca highway, I = VIII ESI-2007; M: tsunami at Salina Cruz, I = VIII ESI-2007. c) enlargement of the coastal area, referring to the 23 June 2020 earthquake. Site I: ground cracks at San Agustín beach, I = X ESI-2007; J: ground cracks at Maguey beach, I = X ESI-2007; K: liquefaction at Copalita river, I = VII ESI-2007; L: liquefaction at Zimatán, I = VII ESI-2007.

Figure 7: DYFI data for the 8 September 2017 (a) and 23 June 2020 (b) earthquakes.

Figure 8. Example of primary effects generated by the 2020 La Crucecita earthquake. a) horizontal ground deformation of 0.43 m NE, San Agustín, Huatulco, Oaxaca (Solano et al., 2020), I = X ESI-2007; b) Tectonic uplift with an estimated vertical movement between 40 - 50 cm (Solano et al., 2020). It is possible to observe the emergence of colonies of Monoplacophore mollusks on pillars due to the raising of the basement level, Santa Cruz, Huatulco, Oaxaca, I = X ESI-2007.

Figure 9. Example of secondary effects generated by the 2020 La Crucecita earthquake. a) Landslide and rockfall, estimated maximum volume of $10^4$-$10^5$ $m^3$, Oaxaca – Tehuantepec highway (Diario Marca, 2020), I = VIII ESI-2007; b) Rockfall with an estimated maximum volume of $10^3$ $m^3$ from unstable slope, San Juan Guivini, Oaxaca (from Rockfall_Guivini, 2020), I = VII ESI-2007; c) Cracking in sandy soil road, 1-20 cm width, Río Hondo, Miahuatlán, Oaxaca (from Cracking_RíoHondo, 2020), I = VI ESI-2007; d) Landslide of $10^3$ $m^3$ approx. in volume, Santo Domingo Ozolotepec, Oaxaca (from Landslide_Ozolotepec, 2020), I = VII ESI-2007; e) Cracking of 1-10 cm width in clay soil road, San Juan Guivini, Oaxaca (from Cracking_Guivini, 2020), I = VII ESI-2007; f) Withdrawal of sea from the coast, prior to the arrival of the tsunami. Ground deformation with 200 m long cracks perpendicular to the sea, Ventanilla Beach, Oaxaca (Velasco et al, 2020; Cracking_VentanillaBeach, 2020), I = VII ESI-2007; g) Sea retreat prior to the arrival of tsunami wave at San Agustín, Huatulco, Oaxaca (Tsunami_Huatulco, 2020), I = VII ESI-2007; h) Measured data (red) and forecast astronomical tide (blue) at the Huatulco station, Oaxaca (from the SMN, 2020), I = VIII ESI-2007.

Figure 10. Top panels: pre-earthquake satellite images; bottom panels: post-earthquake satellite images showing freshly triggered landslides (left panel) and retriggered slides (right panel, landslides marked in the red ellipse).

Figure 11. a) ESI-2007 intensity attenuation for individual subduction zone earthquakes (3 interface and 1 intraslab events) and Intensity Prediction Equation derived for shallow crustal earthquakes in the Italian Apennines (Ferrario et al., 2020); b) Intensity Prediction Equations for MM intensity in the Mexican region for a Ms 7.0 earthquake (Chavez & Castro, 1988).

**Table captions**

Table 1. Parameters of the subduction zone earthquakes used for the analysis of ESI-2007 attenuation; Imax: maximum ESI-2007 degree.

Table 2: Number of documented Intensity Data Points (IDPs) for different EEE types; minimum and maximum distances and the ESI-2007 intensity range are given.

| Date (yyyy/mm/dd) | Locality | Mw | Depth (km) | Type | Imax ESI-2007 | References |
|---|---|---|---|---|---|---|
| 2011/03/11 | Tohoku (Japan) | 9.0 | 29 | Interface | XI | Sanchez & Maldonado (2016) |
| 2016/04/16 | Pedernales (Ecuador) | 7.8 | 21 | Interface | IX | Chunga et al. (2018) |
| 2017/09/08 | Tehuantepec (Mexico) | 8.2 | 46 | Intraslab | IX | This study |
| 2020/06/23 | Oaxaca (Mexico) | 7.4 | 23 | Interface | IX | This study |

| | Type of EEE | N° IDPs | Min-max distance (km) | Description max effects | ESI-2007 range |
|---|---|---|---|---|---|
| **2017 event** | Permanent ground deformation | 2 | 196 – 200 | Subsidence 0.9 m | X |
| | Tsunami | 19 | 127 – 2000 | Runup 3.4 m | V – IX |
| | Landslides | 18 | 165 – 493 | Volume $10^5$-$10^6$ $m^3$ | V – IX |
| | Ground cracks | 7 | 204 – 496 | Length 100s m; throw 70 cm | VI – VIII |
| | Liquefaction and lateral spreading | 6 | 186 – 384 | Length 100s m, width 1 m | VI – IX |
| | Hydrogeological anomaly | 2 | 234 – 350 | Variation in discharge, turbidity | VI – VII |
| | Total affected area | - | - | 200000 $km^2$ | XII |
| | | | | | |
| **2020 event** | Permanent ground deformation | 50 | 2 – 22 | Uplift 0.8 m | IX – X |
| | Tsunami | 9 | 2 – 50 | Runup 1.5 | VII – VIII |
| | Landslides | 42 | 3 – 112 | Volume ca. $10^5$ $m^3$ | V – VIII |
| | Ground cracks | 19 | 2 – 57 | Length 500 m; width 300 cm | VI – X |
| | Liquefaction and lateral spreading | 4 | 7 – 25 | Diameter of sand volcanoes up to 1 m | VI – VIII |
| | Hydrogeological anomaly | 1 | 131 | Water turbidity | VI |
| | Total affected area | - | - | 14000 $km^2$ | XI |

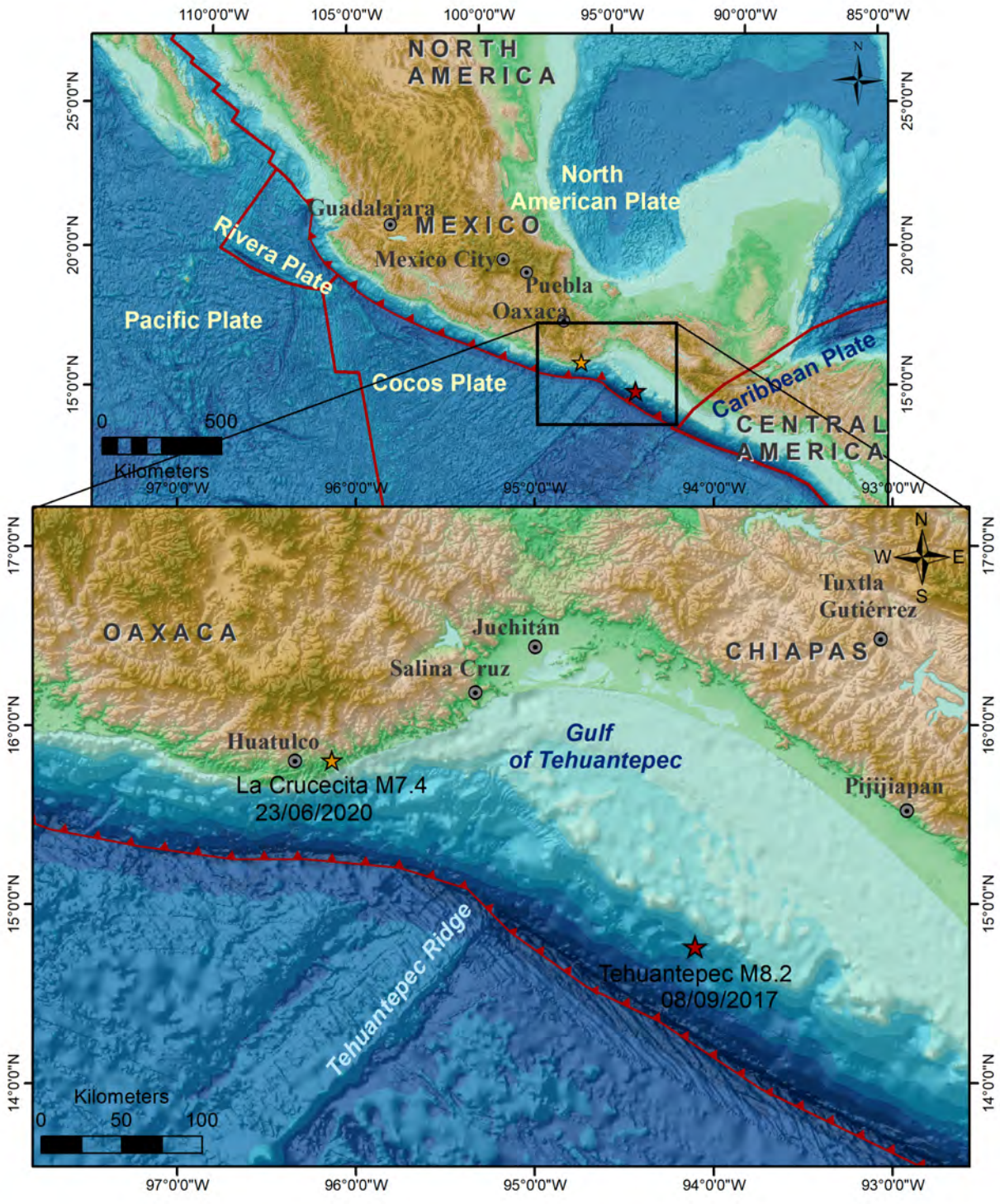
110°0'0"W
105°0'0"W
100°0'0"W
95°0'0"W
90°0'0"W
85°0'0"W
25°0'0"N
20°0'0"N
15°0'0"N
NORTH AMERICA
North American Plate
Guadalajara
MEXICO
Mexico City
Puebla
Oaxaca
Rivera Plate
Pacific Plate
Cocos Plate
Caribbean Plate
CENTRAL AMERICA
0
500
Kilometers
97°0'0"W
96°0'0"W
95°0'0"W
94°0'0"W
93°0'0"W
17°0'0"N
16°0'0"N
15°0'0"N
14°0'0"N
N
W
E
S
Tuxtla Gutiérrez
OAXACA
Juchitán
CHIAPAS
Salina Cruz
Gulf of Tehuantepec
Huatulco
La Crucecita M7.4
23/06/2020
Pijijiapan
Tehuantepec Ridge
Tehuantepec M8.2
08/09/2017
Kilometers
0
50
100

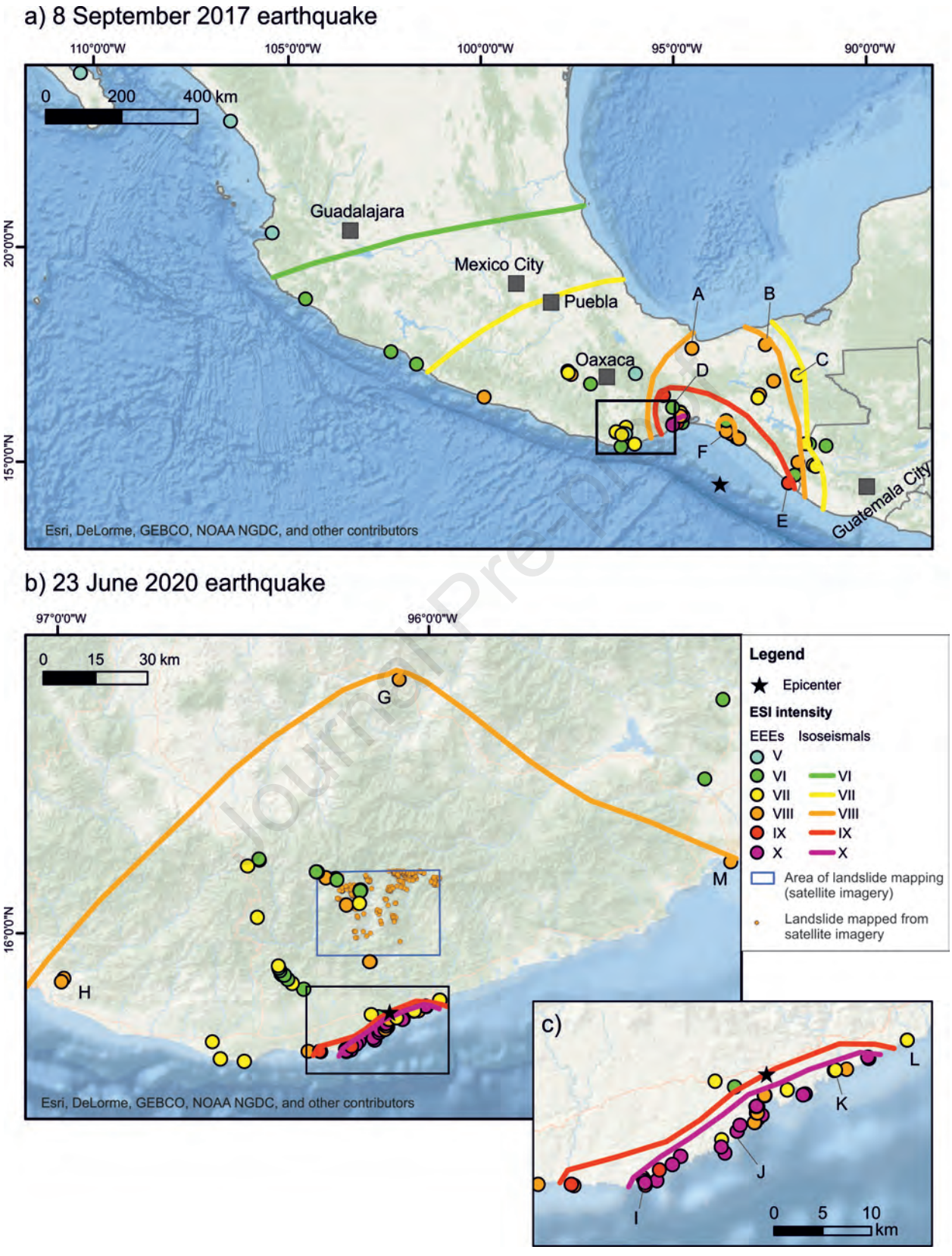
a) 8 September 2017 earthquake
110°0'0"W
105°0'0"W
100°0'0"W
95°0'0"W
90°0'0"W
0
200
400 km
20°0'0"N
15°0'0"N
Guadalajara
Mexico City
Puebla
Oaxaca
A
B
C
D
E
F
Guatemala City
Esri, DeLorme, GEBCO, NOAA NGDC, and other contributors
b) 23 June 2020 earthquake
97°0'0"W
96°0'0"W
0
15
30 km
16°0'0"N
G
H
M
Legend
Epicenter
ESI intensity
EEEs
Isoseismals
V
VI
VII
VIII
IX
X
Area of landslide mapping (satellite imagery)
Landslide mapped from satellite imagery
Esri, DeLorme, GEBCO, NOAA NGDC, and other contributors
c)
I
J
K
L
0
5
10
km

a) 8 September 2017 earthquake

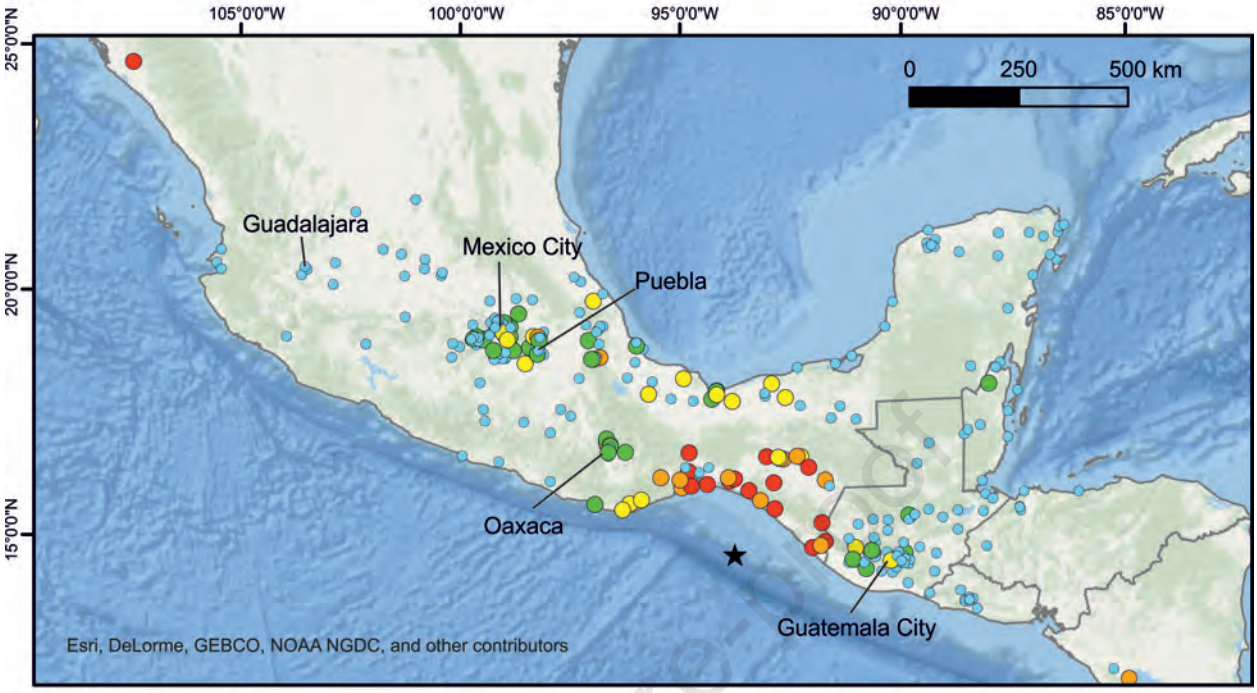


b) 23 June 2020 earthquake

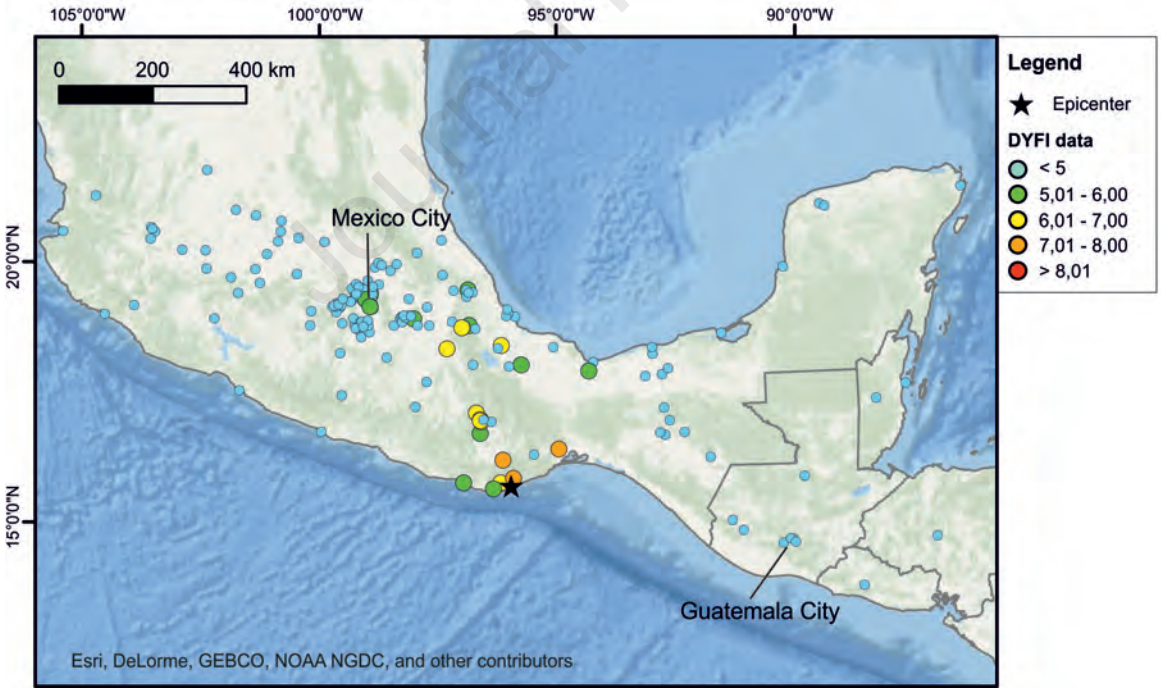

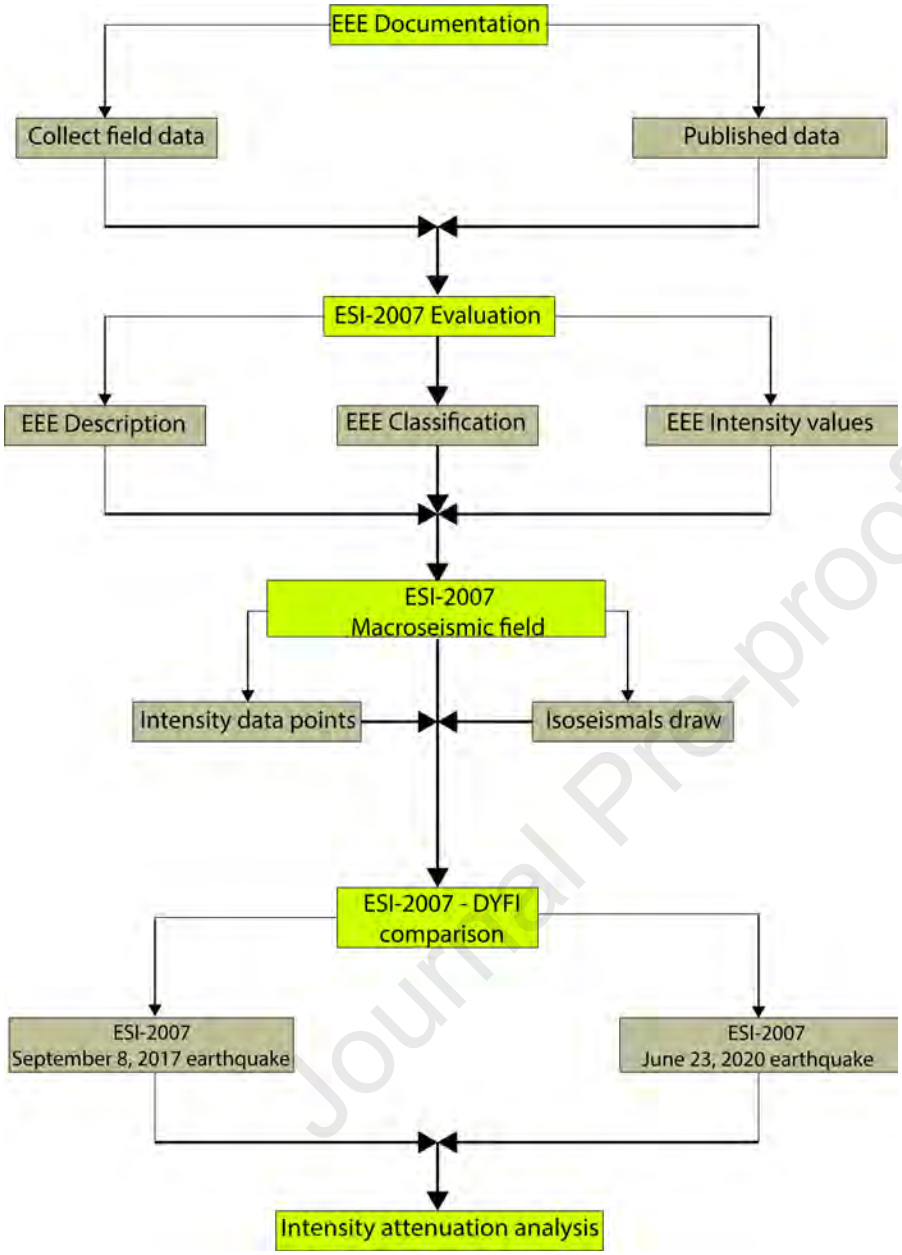

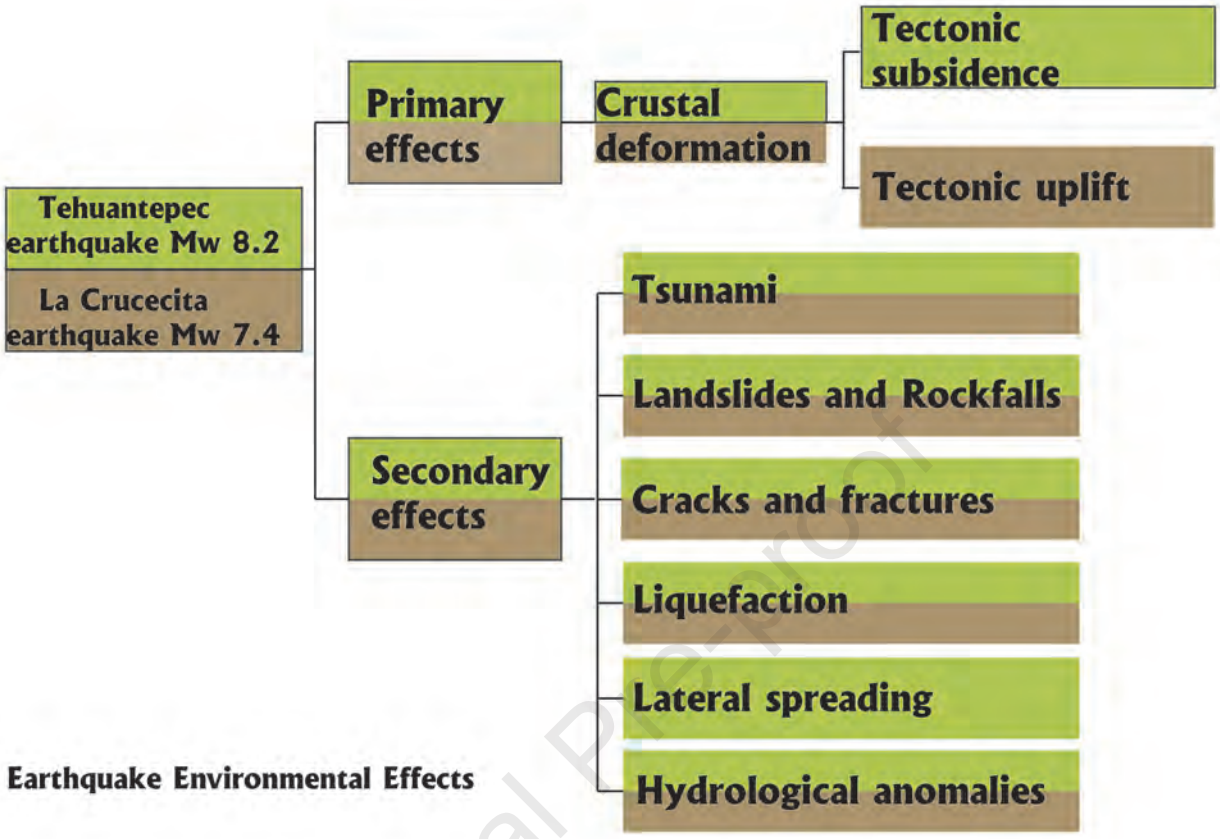




DataCam© Google Play
a
a'


b


c


d


e

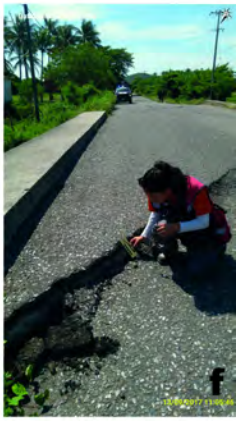
f


Cañón del
Sumidero
g

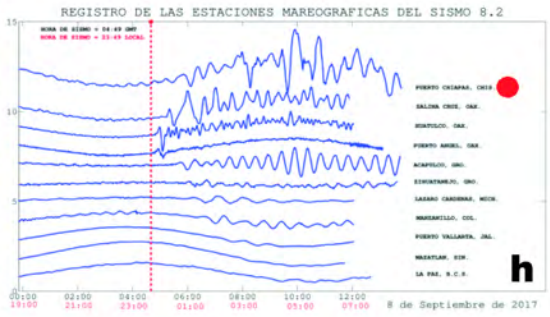
REGISTRO DE LAS ESTACIONES MAREOGRAFICAS DEL SISMO 8.2
8 de Septiembre de 2017
h



a
b
c
d
e
h
f
Drone Huatulco
g

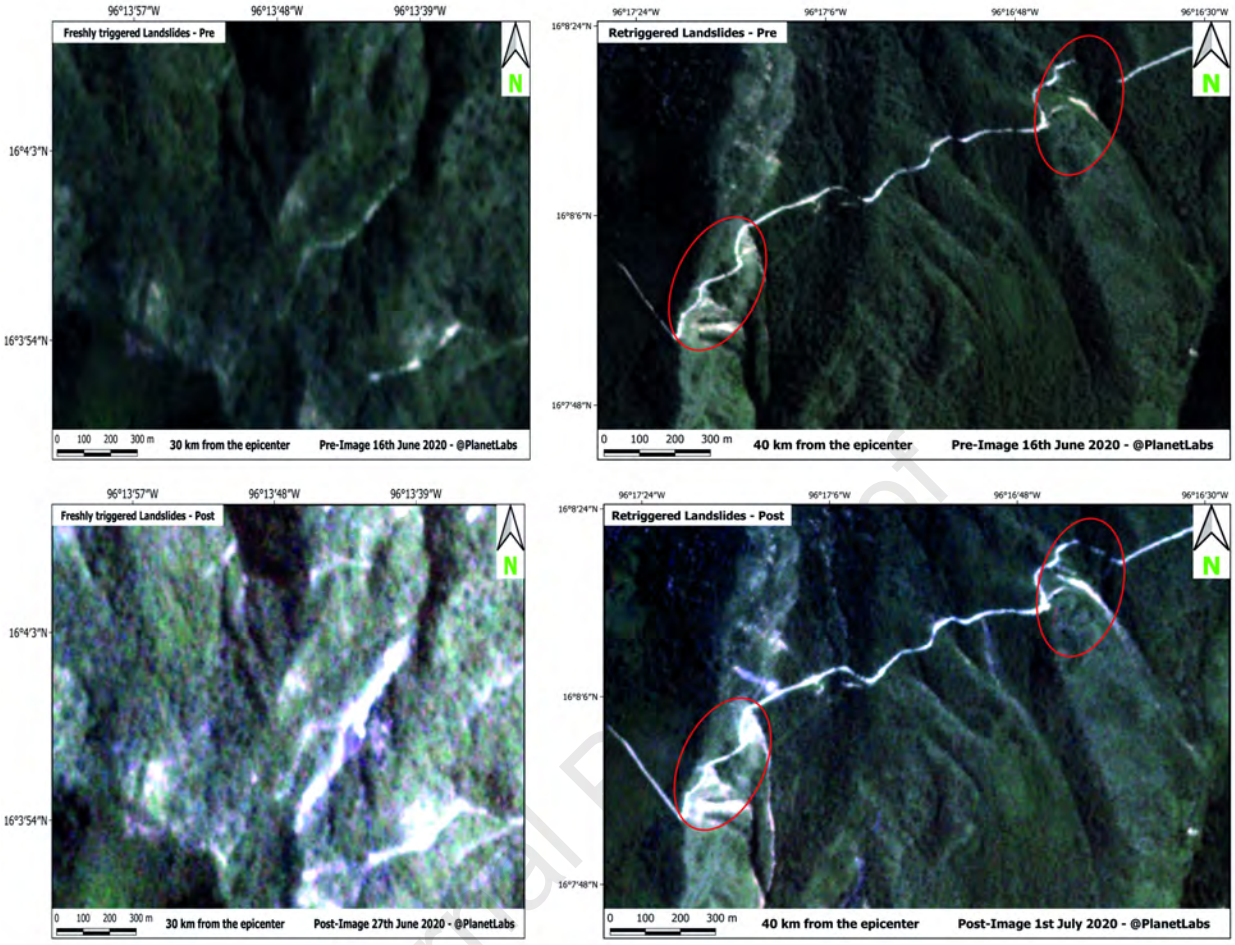
96°13'57"W
96°13'48"W
96°13'39"W
Freshly triggered Landslides - Pre
N
16°4'3"N
16°3'54"N
0 100 200 300 m
30 km from the epicenter
Pre-Image 16th June 2020 - @PlanetLabs
96°17'24"W
96°17'6"W
96°16'48"W
96°16'30"W
16°8'24"N
Retriggered Landslides - Pre
N
16°8'6"N
16°7'48"N
0 100 200 300 m
40 km from the epicenter
Pre-Image 16th June 2020 - @PlanetLabs
96°13'57"W
96°13'48"W
96°13'39"W
Freshly triggered Landslides - Post
N
16°4'3"N
16°3'54"N
0 100 200 300 m
30 km from the epicenter
Post-Image 27th June 2020 - @PlanetLabs
96°17'24"W
96°17'6"W
96°16'48"W
96°16'30"W
16°8'24"N
Retriggered Landslides - Post
N
16°8'6"N
16°7'48"N
0 100 200 300 m
40 km from the epicenter
Post-Image 1st July 2020 - @PlanetLabs

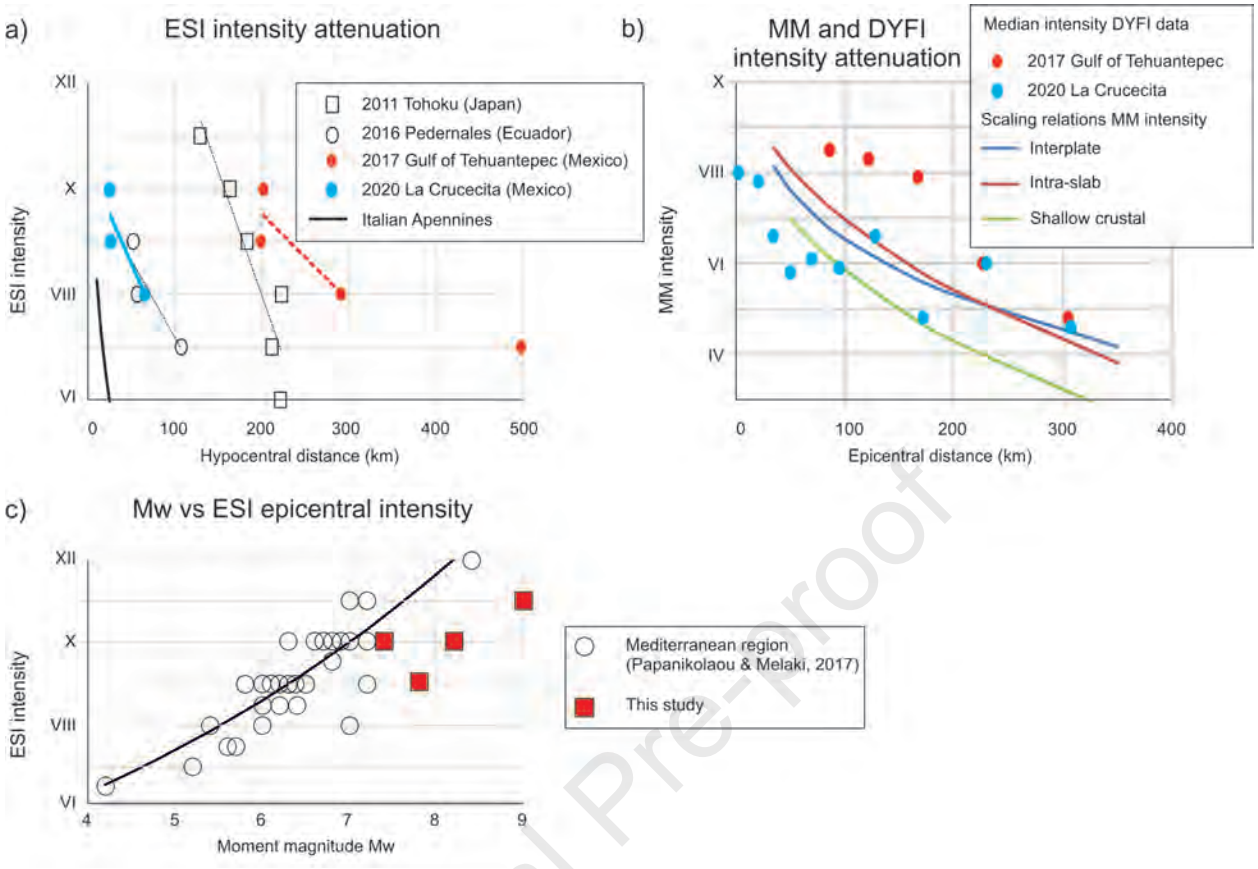

**Declaration of interests**

☒ The authors declare that they have no known competing financial interests or personal relationships that could have appeared to influence the work reported in this paper.

☐The authors declare the following financial interests/personal relationships which may be considered as potential competing interests: